IJST, Transactions of Electrical Engineering, Vol. 37, No. E2, pp 161-182
Printed in The Islamic Republic of Iran, 2013

STATOR TURN-TO-TURN FAULT DETECTION OF SYNCHRONOUS GENERATOR USING TOTAL HARMONIC DISTORTION (THD) ANALYZING OF MAGNETIC FLUX LINKAGE*

H. YAGHOBI[1,**] K. ANSARI[2] AND H. RAJABI MASHHADI[3]

[1]Dept.of Electrical Engineering, Semnan University, Semnan, I. R. of Iran
Email: yaghobi@profs.semnan.ac.ir
[2, 3]Dept. of Electrical Engineering, Ferdowsi University of Mashhad, Mashhad, I. R. of Iran

Abstract– Diagnostics of synchronous generator turn-to-turn faults can be accomplished by analyzing the anomalies of machine local variable such as magnetic flux linkage. On the other hand, because current transformers and voltage transformers are usually installed in the machine for different purposes as default, the monitoring schemes that depend on the study of these inputs have become a topic of interest. As a consequence, in the last two decades, a variety of methods have been proposed based only on the global external variable (such as stator current and voltage). It must be noted that the global external variable analysis techniques are not capable of detecting all of the potential faults in electrical machines and some researches, including this work, aim to transfer a part of the global external variables analysis knowledge to techniques that monitor the signatures produced by the fault to the electromagnetic flux signals (local variable). Hence, this contribution deals with the analysis of the stator turn-to-turn short circuit fault of salient-pole synchronous generator. In this paper, a fault indicator based on harmonic analysis of the magnetic flux linkage is investigated. Experimental results derived from a 4-pole, 380V, 1500 rpm, 50 Hz, 50 KVA, 3-phase salient-pole synchronous generator, show that the proposed method is useful and effective.

Keywords– Synchronous generator, inter-turn fault, magnetic flux linkage, harmonic analysis

1. INTRODUCTION

Recently, monitoring methods for electrical machines have become a matter of importance [1]. Condition monitoring of electrical machines could prevent tragic losses and prepare a precise view of machine operation. On the other hand, synchronous generators are the basic and significant elements of power systems [2] and their failure can cause severe damage to the machine, interruption of electrical supply, and ensuing economic loss. Therefore, it is very important to have a careful analysis of the internal faults in synchronous generators to increase their useful life and reliability. Hence a reliable and accurate diagnosis of the internal faults is a challenging problem in the area of fault diagnosis of electrical machines. The purpose of this study is to achieve greater efficiency in fault detection and to provide a reliable method with low-cost sensors and simple numerical algorithms which not only detects the occurrence of the fault, but also locates its position. However, the behavior of the synchronous machine under internal faults has not been thoroughly studied [3] and machine fault diagnostics still constitute an open problem [4]. The expertise in this field is still in permanent evolution and new methods appear every year. There have been significant investigations of fault diagnostics during the last decade and different methods have been developed. Because current transformers and voltage transformers are usually installed in the machine for

*Received by the editors September 1, 2012; Accepted November 26, 2013.
**Corresponding author

different purposes as default, the monitoring schemes that depend on the study of these inputs (global external variables) are mostly of interest. As a consequence, a variety of methods are proposed based only on the global external variables such as stator current and voltage [5]-[8]. On the other hand, taking into consideration the following possible problems of a condition monitoring system relying only on current signature analysis, the stimulus for approaching and relying on additional fault indicators seems to be obvious and pragmatic [9]-[11]:

- For various faults, current signature analysis may not provide sufficient ability to diagnose faults at their inception and discriminate between different hybrid faults, since such abnormalities and time harmonics may end up generating similar signatures.
- The current spectrum is influenced not only by fault situations but also by other causes, containing the supply, static and dynamic load conditions, noise, machine geometry, and fault conditions, and these situations may lead to mistakes in fault detection.
- When a commercial fault detection system has to work under a range of diverse designs and driving an extensive range of mechanical loads, providing a diagnosis from sensing only the current and its subsequent analysis becomes much more difficult than is at first apparent.
- In order for reliable and successful detection of faults during steady state operation, a large supply of current is required. For this large current, the machine must be operating at or near full load conditions. On the other hand, there are special situations that the machine must only be tested under no-load conditions and load operations are not available.
- It is important to bear in mind that the current signature analysis techniques are not capable of detecting all of the potential faults in electrical machines.

Table 1. Potential measurement parameters and fault indicators in electrical machines [12]

Parameter	Measurement device	Potential information richness	On/Off line	Intrusive to electrical machine	Operator skill required
Current	Hall Effect transducer	Average	On	No	High
Voltage	DVM	Average	On	No	High
Flux	Search coil	Very high	On	Yes and No	High
	Hall effect device				
Force	Dynamometer	Very high	On	No	High
Vibration	Accelerometer	High	On	Yes and No	Expert
Acoustics	Microphone	High	On	No	Expert
Temperature	Hand-held probe	Low	Off	Yes and No	Low
	Thermal paint			Yes	
	Thermocouple	Average	On	Yes	Average
	Infra-red camera	High		No	Expert
Instantaneous angular speed	Encoder	Average	On	No	High
Torque	Torque sensors (magneto elastic, piezo electric,strain gauge)	High	On	No	Expert

On the other hand, Payne et al. [12] briefly compared the different types of fault diagnosis system in transverse flux motor that is presented in Table 1. Their results showed the monitoring devices which rely on the electromagnetic flux as a local variable had very high accuracy. Even though the content of this research refers to a transverse flux motor, which is not typical of industrial drives, this may also be considered as being representative of any kind of electrical machine, since the same potential measurement parameters are presented by other researches as likely to provide useful condition-indicating information for possible fault modes [9]. In this respect, some studies [9], [13]-[20], including this work, were aimed to transfer a part of the current signature analysis knowledge to techniques that monitor the signatures generated by the fault to the magnetic flux signals. Hence, as a recent trend, fault monitoring of rotating electrical machines using magnetic field measurements have been proposed as a common subject of investigation [17], [18]. In this paper, a fault indicator based on harmonic analysis of the magnetic flux linkage for the diagnosis of turn-to-turn winding fault in a salient-pole synchronous generator is presented. Also, probabilistic neural network (PNN) and discrete wavelet transform (DWT) are used in design of fault diagnosis system. PNN as the main part of this fault diagnosis system and DWT are combined effectively to construct the classifier. In this contribution, DWT is used only for de-noising, because by reducing the noise, better network training is done. The main feature of the proposed method is that it is capable of identifying the faulty coils under winding faults. Simple algorithm, low cost sensor and sensitivity are other features characterized by the proposed technique. In this method, the generator air gap flux linkage is measured via search coils sensor installed under the stator wedges inside the machine. This sensor is readily accessible on the market and its cost is very low.

2. EFFECTS OF INTERNAL FAULTS ON THE MAGNETIC FLUX DISTRIBUTION

Early stages of internal faults in stator winding often have insignificant effects on the machine performance; however, such faults may quickly lead to considerable faults and subsequently destructive failures [4]. Undetected turn-to-turn faults produce heat in the deformed region of a winding which finally develop and change into phase-to-ground or phase-to-phase faults [21].

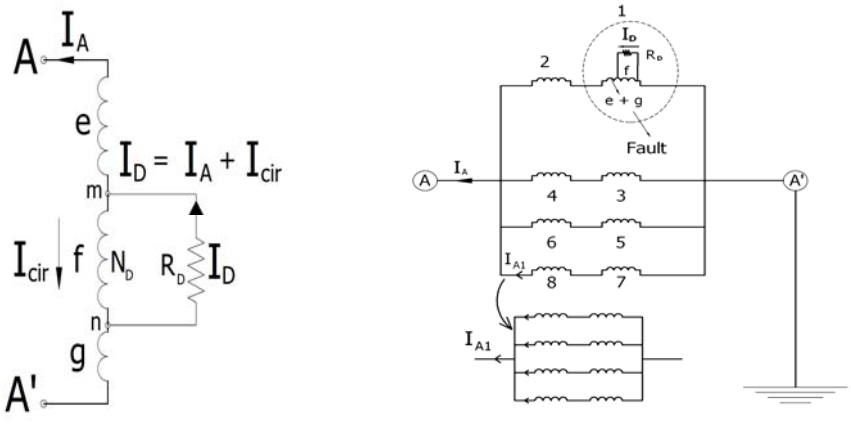

(a) (b)

Fig. 1. (a) Inter-turn short circuit between two points, *m* and *n* [9]. (b) The arrangement of stator winding (phase A) with star connection during turn-to-turn short circuit in the same branch

This type of fault is a major reason for the stator winding failures and other faults may result from it [21]. In addition, a severe fault such as a phase-to-ground fault may lead to irreversible damage to the stator winding and core [4]. Therefore, it is very important to analyze and detect stator inter-turn faults at an early stage to prevent further damage to the machine and involved systems. When inter-turn short

circuit occurs, the short turn will act as the secondary winding of an autotransformer (see Fig. 1b). Consequently, a very large circulating current will flow in the faulted turn. This circulating current causes excessive heat and high magnetic forces in machine [22]. Figure 1a illustrates the case when a turn-to-turn short circuit has occurred in the same branch between two points, m and n. Also, Fig. 1a shows that two currents produce opposite MMFs, one of which is the phase current (I_A) and the other is the short circuit current (I_D) (The difference between these two currents is defined as circulating current I_{cir}).

Therefore, the main effect of the inter-turn short circuits decreases the MMF close to the short-circuited turns [23]. Under ideal conditions, the machine has an air-gap magneto-motive force which varies sinusoidally in space and time. Faulty operation will cause a distortion in the air-gap magneto-motive force of the machine. Fig. 2a and b show the typical magnetic flux distribution under normal and turn-to-turn fault in stator winding of the studied generator as obtained by the finite element method (FEM).

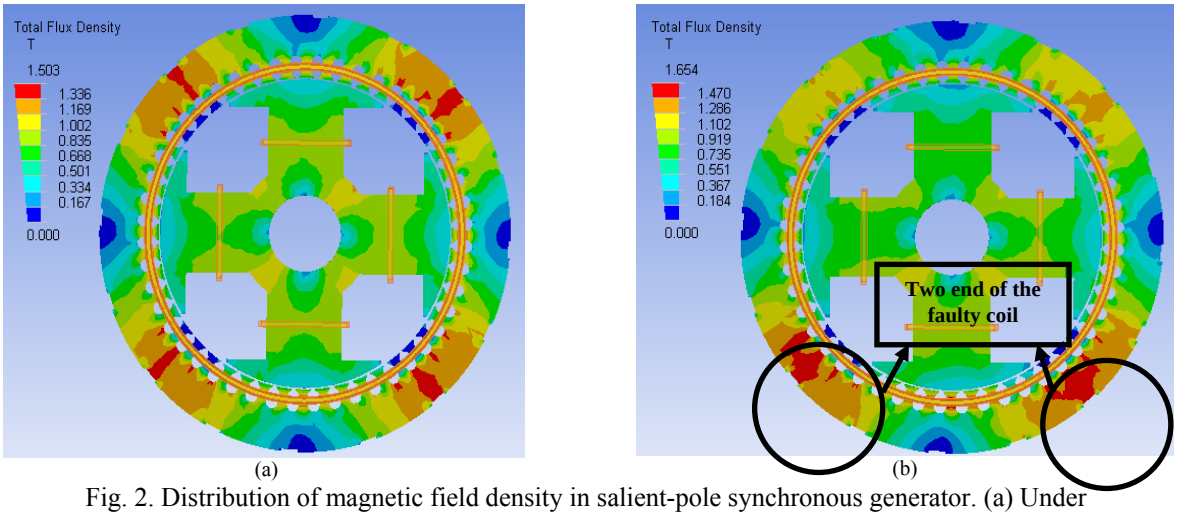

(a) (b)

Fig. 2. Distribution of magnetic field density in salient-pole synchronous generator. (a) Under healthy operation. (b) Under inter-turn short circuit in stator winding

In Fig. 2a magnetic flux distribution varies from 0.167T (q-axis) to 1.503T (d-axis). Figure 2b illustrates flux distribution under turn-to-turn fault. In this figure, magnetic flux distribution varies from 0.184T to 1.654 T. Due to the high circulating current in the fault areas, magnitude of magnetic flux linkage under fault condition in these areas is higher than the normal case (see Fig. 9). Also, Figs. 3a and b show the typical magnetic flux line under normal and turn-to-turn fault in stator winding of the generator. It is evident from both figures that magnetic field distribution and magnetic flux line in synchronous generator under healthy operation is symmetric. But when a turn-to-turn fault occurs, this fault will cause nonsymmetrical distribution of magnetic flux linkage. Therefore, magnetic flux linkage is a suitable criterion for the detection of the turn-to-turn faults in synchronous generator. In fact, in electrical machines, air-gap magnetic field distribution in no-load and on-load performance under normal conditions is symmetric (neglecting the insignificant inherent asymmetry in the magnetic field distribution due to the differences in the mechanical structures). But this symmetry is especially lost under internal fault occurrences.

On the other hand, Figs. 4 and 5 show the typical torque, current and induced voltage in different phases under normal operation and turn-to-turn fault in stator winding of the studied generator as obtained by the finite element method (FEM). The simulations indicated the difficulty of finding clear fault signatures based only on the global external variables (such as stator current, voltage and torque). These methods (based on analysis of the global external variables) have the obvious advantage of simplicity but also the drawback of low sensitivity, especially in an early stage of a fault [24]. It must be noted, the

simulations in this research have been done in both environments, i.e. magneto-static and transient mode by using two types of software (Maxwell and ANSYS workbench software).

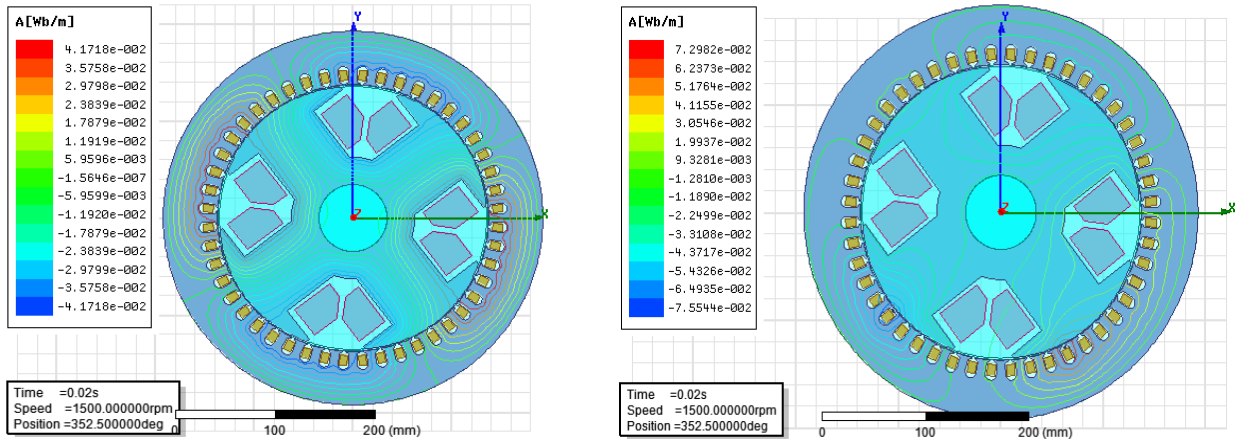

(a) (b)

Fig. 3. Magnetic flux lines of complete view in salient-pole synchronous generator. (a) Under normal operation. (b) Under inter-turn short circuit in stator winding

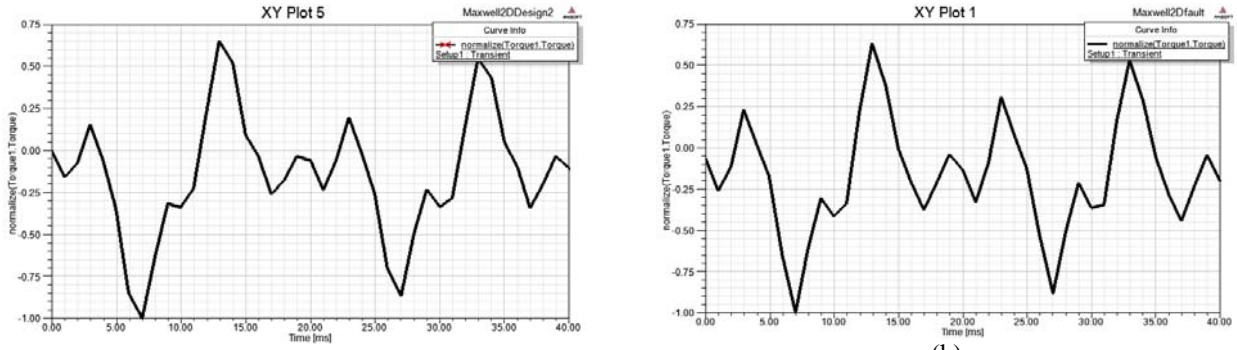

(a) (b)

Fig. 4. Torque. (a) Under normal operation. (b) Under inter-turn short circuit in stator winding

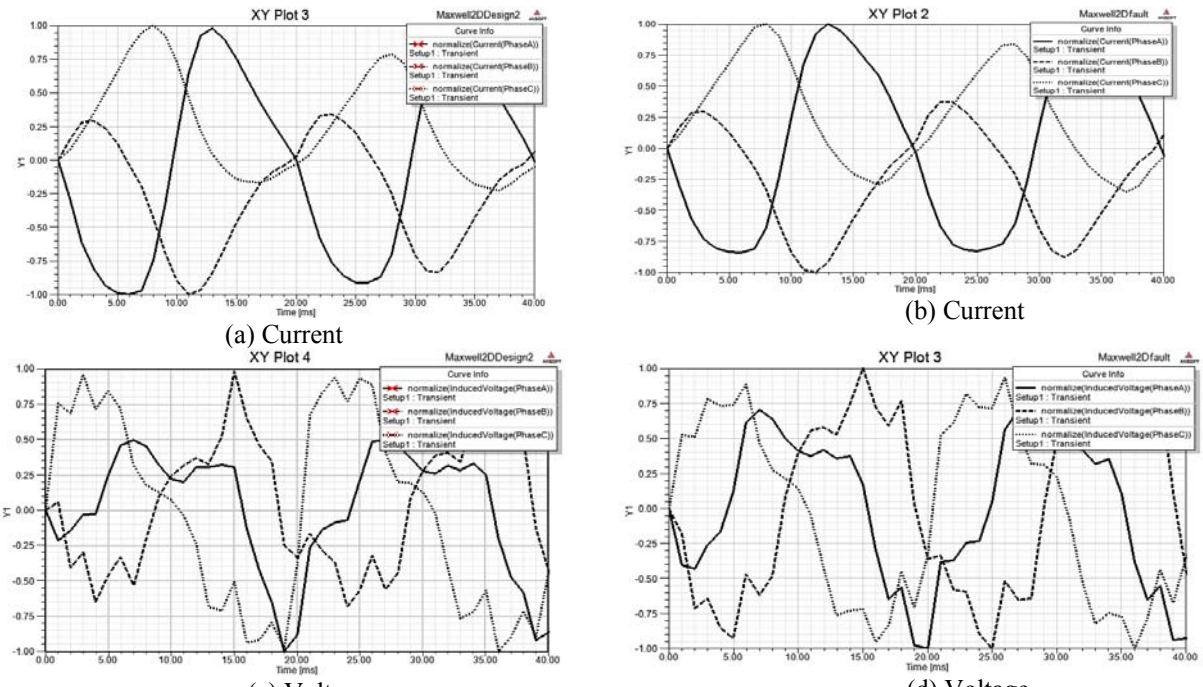

(a) Current (b) Current

(c) Voltage (d) Voltage

Fig. 5. Currents and voltages in different phases. (a) and (c) under normal operation. (b) and (d) under inter-turn short circuit in stator winding

3. EXPERIMENTAL TEST SETUP AND MEASURING TECHNIQUE

In this section, the performance of the mentioned generator under different operation conditions is explained.

a) Experimental test setup

The machine used in this study is a 50 KVA, 380V, 4-pole, 1500 rpm, 50 Hz, 48 stator slots, salient-pole synchronous generator. The stator of this generator has a 3-phase, one layer, lap winding, and four parallel branches in each phase. Testing laboratory and experimental test setup are shown in Fig.6.

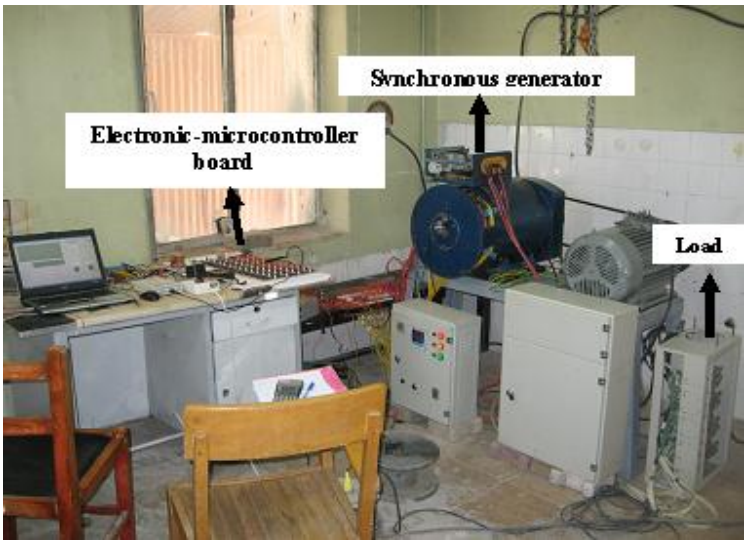

Fig. 6. Testing laboratory and experimental test setup

It consists of a synchronous generator connected to a three-phase resistive load. This generator has no damper winding, and is driven by an induction machine. In fact, a usual commercially accessible generator was disassembled and in order to produce turn-to-turn fault, isolation of the few turns from the same coil was damaged. At these points, some conductors were soldered and taken out of the machine. Short circuit was made between these conductors. Thus, turns were shortened externally. By measuring the EMF between these conductors and being aware of winding details, we were capable of deducing how many turns in one coil were shortened. Several of the internal faults were performed on the mentioned generator under different conditions. Measurements at full excitation current were carried out under normal condition. However, because of the major concern over testing machine health for further tests, measurements at full excitation current were not carried out under faulty condition.

Through the experiments performed in this work, search coils and designed electronic-microcontroller board are used for measuring simultaneously flux linkage data in cross-section of the aforementioned generator. Designed electronic-microcontroller board has one master and forty eight slaves. Serial port interface has been used for connecting the designed electronic-microcontroller board to the computer. The induced voltages in the search coils are transferred to the serial port of the computer by means of the designed electronic-microcontroller board. Schematic and experiment view of these used search coils are illustrated in Fig.7. These inductive sensors observe the real distribution of the air-gap flux density. This indicates that all damping effects coming from the saturation and the parallel current branches of the stator winding are taken into account. This sensor is readily accessible on the market and its cost is very low compared with capacitive air-gap monitoring system [14], [25].

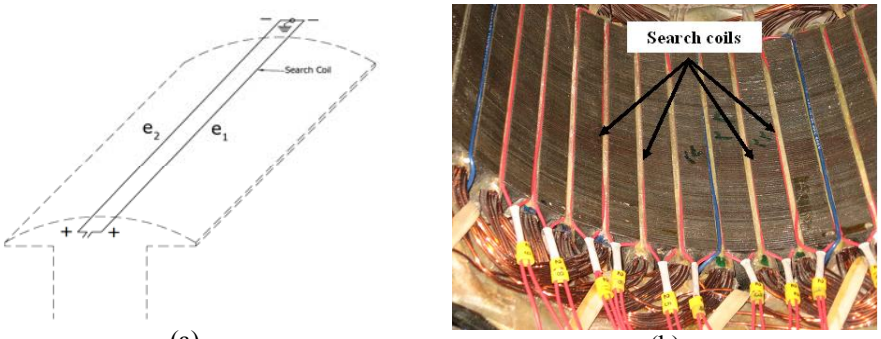

(a) (b)

Fig. 7. (a) Schematic view of search coil. (b) Search coils placed along the stator teeth in experiment to detect short-circuit faults

Easiness and low price of the used inductive sensors allow the installation of a high number of sensors [25]. Hence, in order to improve the accuracy, in this research, forty eight single turn search coils were installed along the grooves of the stator teeth with a pitch of 15° with the aim of being able to determine how the flux linkage distribution in the generator changes when an abnormal operational condition is present. Also, this sensor has more advantages such as insensitivity to external conditions (humidity, temperature, etc.) and no need for mechanical disassembling / reassembling.

It must be noted that, condition monitoring needs the sensing and analysis of such signals that include specific information which is characteristic of the degradation process, problem, or fault to be detected. A variety of factors must be considered when choosing the most suitable monitoring method for application in an industrial environment. In the following, the most significant factors [9], [10] are listed:

1. The sensor should be non-invasive,
2. The sensor and instrumentation system must be reliable,
3. The diagnosis must be reliable,
4. The severity of the problem should be quantified,
5. Ideally, an estimation of the remaining run-life should be given,
6. Ideally, a prediction of the fundamental cause(s) of the fault should be provided via online information from sensors etc.

It is very difficult and, in most cases, impossible to gratify all the criteria, mainly because of the complexity of the degradation mechanisms, abnormalities, and the nature of the fault [9], [10].

b) Total harmonic distortion

The total harmonic distortion (THD) can be represented by several different methods. In one of the most common, the THD is defined as the root mean square (RMS) value of the total harmonics of the signal, divided by the RMS value of its fundamental signal. For example, for signal X, the THD or harmonic factor is defined as:

$$THD = \frac{X_H}{X_F} \tag{1}$$

Where $X_H = \sqrt{X_2^2 + X_3^2 + \ldots + X_n^2}$

X_n : RMS value of the harmonic n

X_F : RMS value of the fundamental signal

c) Different operation conditions and loading effect

The induced voltage in the sensors under different operation conditions and loading effect are explained in this subsection. Frequency analysis is the process of determining the frequency

domain representation of a time domain signal and most commonly employs the fast Fourier transform (FFT). The FFT allows specifying the desired output format, to specify a frequency of interest, and to obtain any number of harmonics as well as the total harmonic distortion. In this research, FFT is used to extract the fault signature from magnetic flux linkage and a fault indicator based on THD is presented.

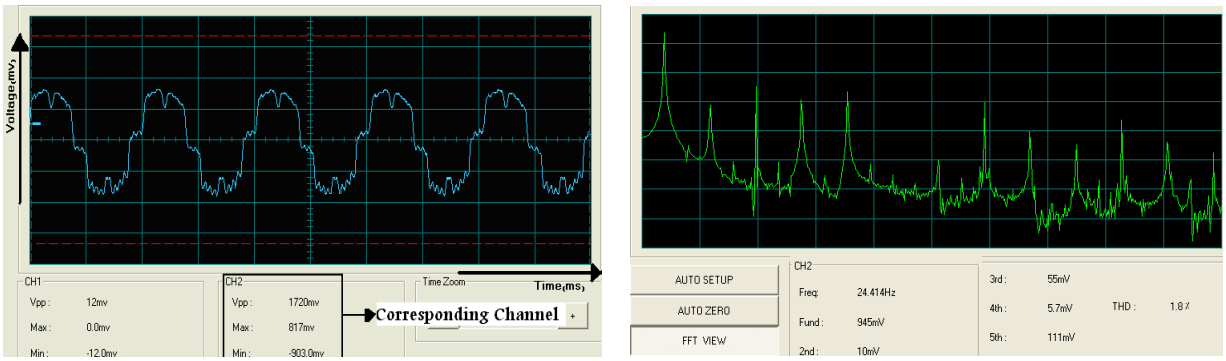

(a) (b)

Fig. 8. Under healthy operation at no-load. (a) Measured flux linkage. (b) Frequency spectrum of flux linkage

Figure 8a shows the measured magnetic flux linkage induced in a search coil, under healthy operation at no-load. According to this figure, it can be seen that, under ideal conditions, the machine has an air-gap magnetic field which varies sinusoidally in space and time. Its frequency spectrum is shown in Fig. 8b. Also, Fig. 9a shows the measured magnetic flux linkage induced in a search coil, under faulty operations at no-load and its frequency spectrum is shown in Fig. 9b. According to this figure, it can be seen that, faulty operation will cause a distortion of this sinusoidal waveform. Due to the high circulating current in the fault areas, magnitude of magnetic flux linkage under fault condition in these areas is higher. Comparing Fig. 8b and Fig. 9b, the THD increases from 1.8% to 25.7% after the fault has happened. This large increase in the THD that indicates the fault has occurred. Therefore by analyzing magnetic flux linkage of the machine, inter turn faults can be detected. In fact, a fault indicator based on harmonic analysis of the magnetic flux linkage is achieved.

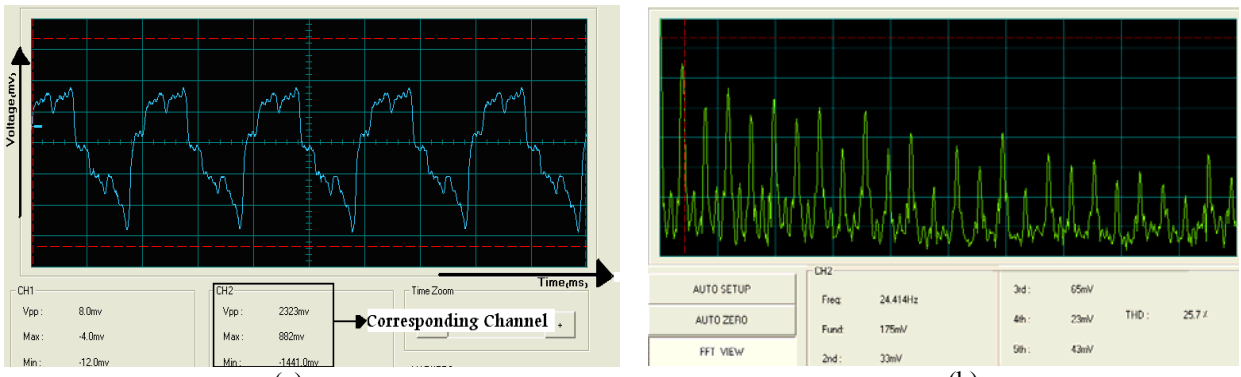

(a) (b)

Fig. 9. Under faulty operation at no-load. (a) Measured flux linkage.
(b) Frequency spectrum of flux linkage

1. Saturation effect:

Because the pitch coils of these search coils are very small, the different saturation level will not significantly affect the general nature of the induced voltage in a search coil.

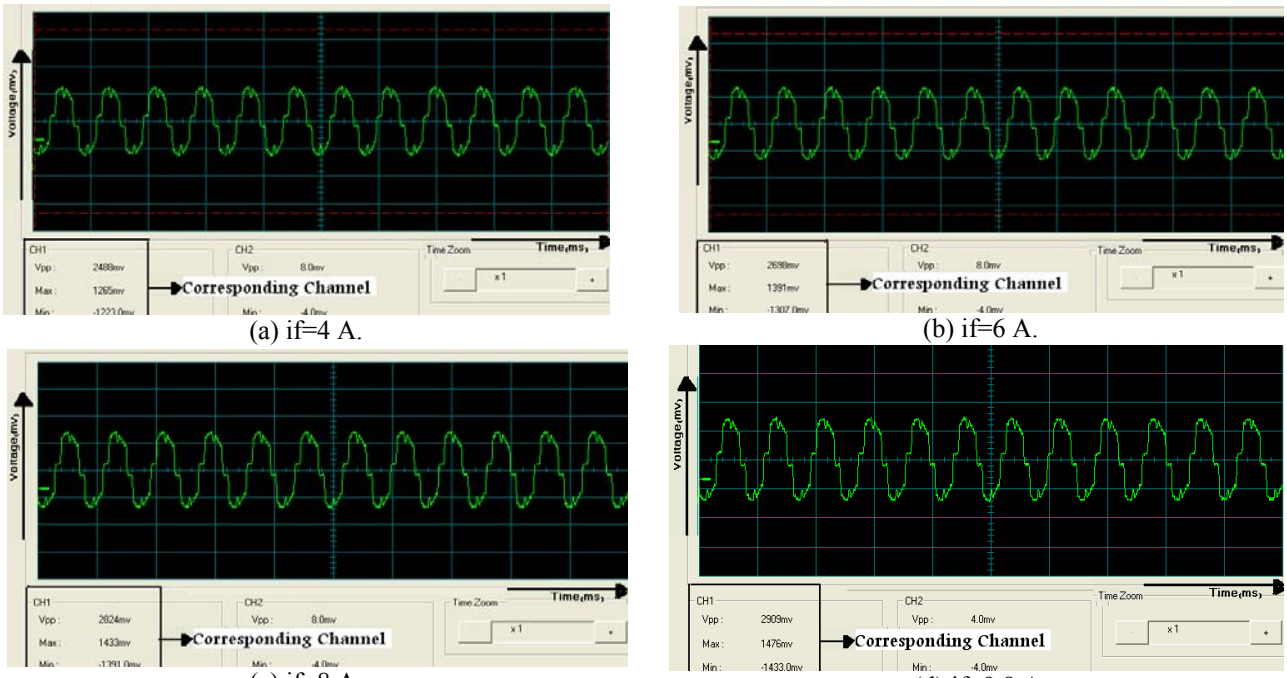

(a) if=4 A. (b) if=6 A.

(c) if=8 A. (d) if=9.8 A.

Fig. 10. Measured induced voltage in a search coil under different excitation current in the normal operations

Figure 10 illustrates the no load voltage induced in a search coil, as the rotor current increases with no fault present in experiment. A field current of 9.8 A represents extreme saturation. According to this figure, the different saturation level will affect the magnitude of the induced voltage in search coils proportional to machine no load curve. In fact, when the rotor current increases, nature of the induced voltage in a search coil at different saturation level is stable and does not change substantially.

On the other hand, frequency spectrum of Fig. 10d (A field current of 9.8 A represents extreme saturation) is shown in Fig. 11. In this condition, there is a slight increase in THD and it increases from 1.8% (under healthy operation) to 2.4% after the extreme saturation has happened.

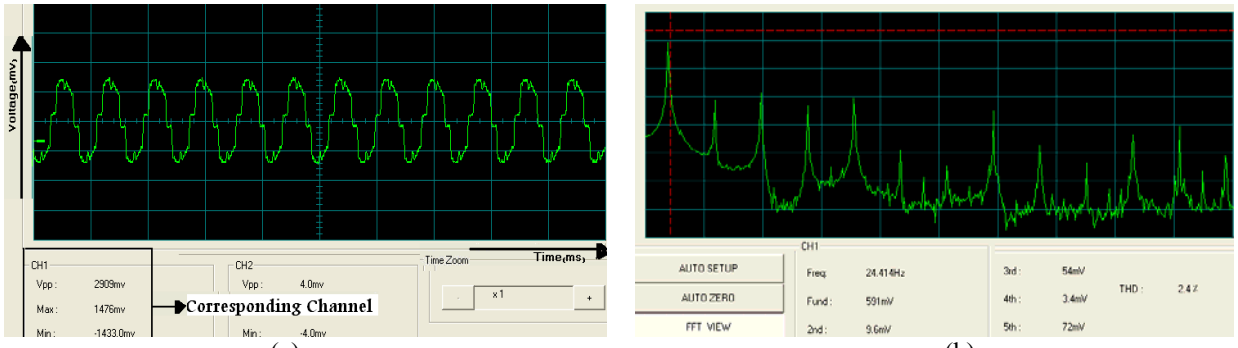

(a) (b)

Fig. 11. Under extreme saturation condition. (a) Measured flux linkage.
(b) Frequency spectrum of flux linkage

2. Loading effect:

Due to limitation in the power of the induction machine, generator has been loaded up to a maximum of around 25% of the rated load in experiment. Although the influence of load level on the detection procedure might seem a drawback, experimental tests showed it is possible to make a reliable diagnosis.

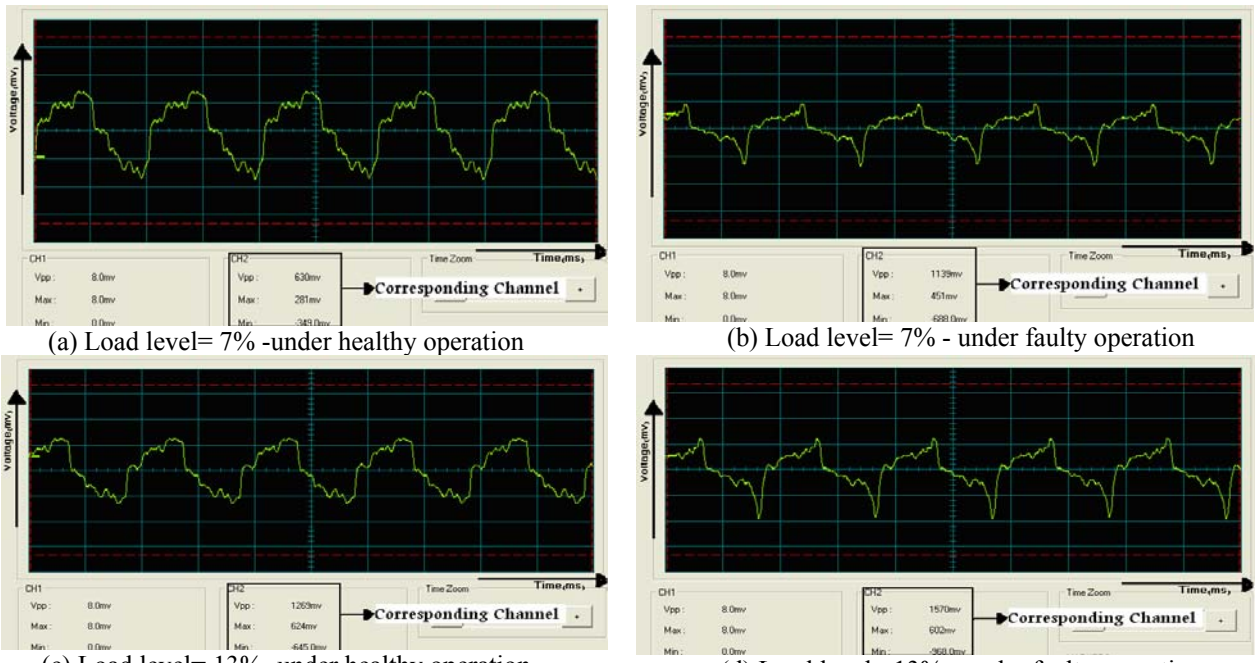

(a) Load level= 7% -under healthy operation (b) Load level= 7% - under faulty operation

(c) Load level= 13% -under healthy operation (d) Load level= 13% - under faulty operation

Fig. 12. Induced voltage in the 31st search coil under different on-load conditions in the normal and faulty operations

Figure 12 shows induced voltages in a search coil, under different on-load conditions in the normal and faulty operations. As it is seen in this figure, the generator load level does not have a major influence on the performance levels of the method.

For better comparison, Fig. 13a shows the induced voltage in a search coil, under healthy operation in no-load and load condition. On the other hand, Fig. 13b shows the induced voltage in a search coil, under inter-turn short circuit in stator winding and healthy operation in no-load. According to Fig. 13a due to the effect of the armature reaction, under on-load conditions, induced voltages in the search coils deviate slightly from the induced voltages in the search coils under no-load conditions. But according to Fig. 13b, under fault condition, induced voltage (sinusoidal waveform) in a search coil is distorted.

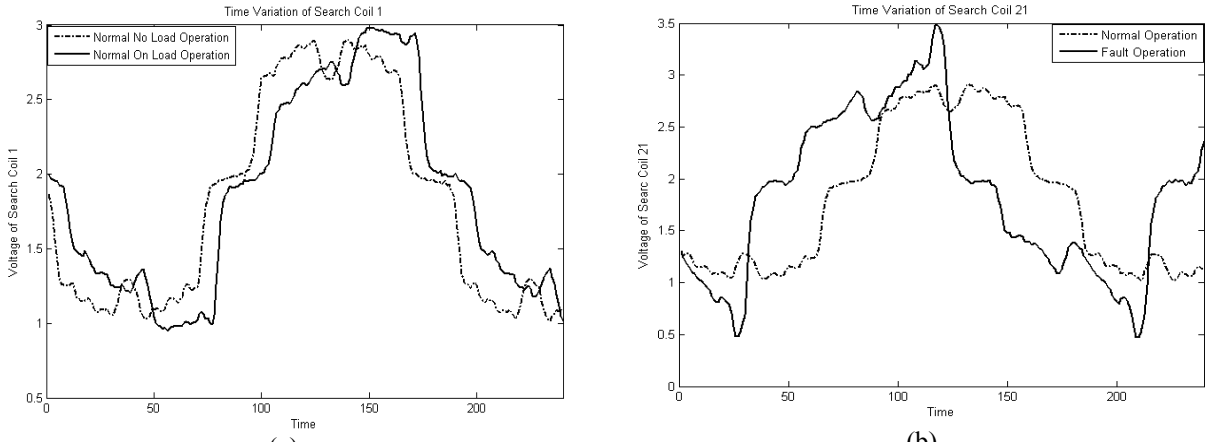

(a) (b)

Fig.13. Induced voltage in a search coils (a) under healthy operation in no load and load condition (b) under inter-turn short circuit in stator winding and healthy operation in no-load

Also, Fig. 14a shows magnetic flux linkage induced in a search coil, under 13% rated load in the normal operation. Its frequency spectrum is shown in Fig. 14b. As is seen in these figures, the generator load does not have a major influence on the performance of the method. Comparing Fig. 8 and Fig. 14, the

THD increases from 1.8% to 6.5% after the load condition has happened. In fact, in this condition, there is not a large increase in THD.

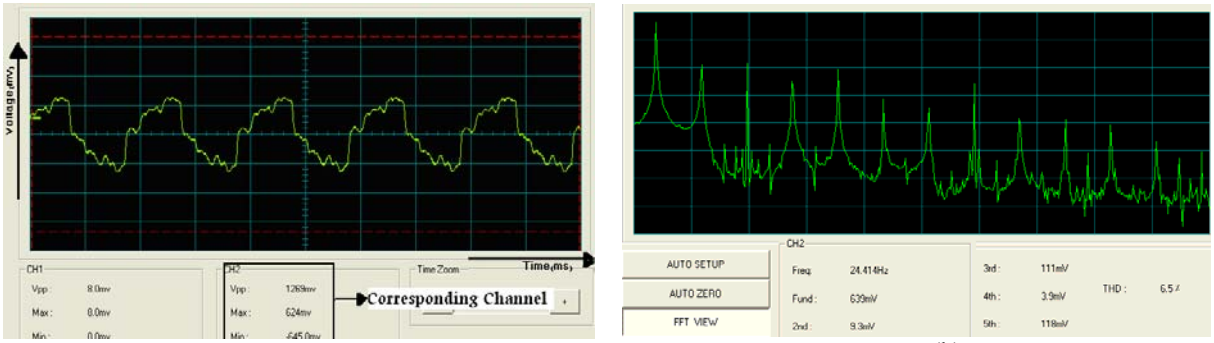

(a) (b)

Fig. 14. Under load condition. (a) Measured flux linkage under healthy operation. (b) Frequency spectrum of flux linkage

On the other hand, Fig. 15 indicates how the armature reaction affects the rotor-produced flux (φ_F) for three power factor (PF) conditions: unity, leading, and lagging. In this figure φ_{ar} is stator produced flux and φ_{ag} is the resultant magnetic flux that rotates at synchronous speed. It is evident from this figure, that unity power factor condition (resistive load) gives maximum deviation under normal operation [14]. It is worth nothing that, in a p pole, healthy, symmetrical machine, the magnetic axis of each pole is located at 360/p geometrical degrees [26]. Under load conditions, the pole axis is not an axis of symmetry, whereas in no-load conditions the pole axis is axis of symmetry. In fact, when a generator is delivering power to the load, the axes of symmetry of the magnetic field deviates from the polar and interpolar axes [27].

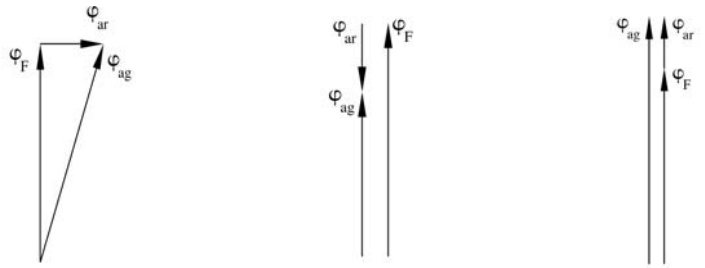

(a) (b) (c)

Fig. 15. Armature reaction for different power factor. (a) PF=1. (b) PF lagging. (c) PF leading [14]

d) Comparative analysis

In order to validate the proposed method, a comparative analysis was made between the proposed method and another similar approach. For identifying the performance of the method, different loading conditions with different percentages of shorted stator windings were used in simulation and experiment and the results are presented in Tables 2-4. The machine stator current and local magnetic flux linkage is used as source signal for fault detection and fault features present in these signals are obtained by THD and negative sequence components analyzing. In fact, for the operation under stator winding short circuits, the THD and negative sequence components of both stator current and magnetic flux linkage will be observed, in order to determine which is the most accurate for fault detection. It must be noted because of the existence of stator flux linkage in d-q axes, the negative sequence component in the stator flux linkage cannot exist alone. Hence, the negative sequence component in the output voltage is calculated equivalent to the negative sequence component in the total stator flux linkage [28].

Table. 2-No load

Source signal	THD						Negative sequence					
	Without fault	With fault (different percentages of fault)					Without fault	With fault (different percentages of fault)				
		2%	4%	6%	8%	10%		2%	4%	6%	8%	10%
Current	1.5%	1.51%	1.51%	1.53%	1.53%	1.54%	0	0.4A	0.6A	0.7A	0.75A	0.85A
Local flux linkage	1.7%	14%	16%	25%	28%	30%	0.25 V	0.26 V	1.7 V	2 V	2 V	2.1 V

Table. 3-Load-13%

Source signal	THD						Negative sequence					
	Without fault	With fault (different percentages of fault)					Without fault	With fault (different percentages of fault)				
		2%	4%	6%	8%	10%		2%	4%	6%	8%	10%
Current	1.52%	1.521%	1.53%	1.52%	1.52%	1.55%	0	0.4A	0.62A	0.73A	0.76A	0.87A
Local flux linkage	6.5%	18.5%	22%	30%	35%	36.5%	0.38 V	1.8 V	2.1 V	2.2 V	2.2 V	2.3 V

Table. 4-Load-100%

Source signal	THD						Negative sequence					
	Without fault	With fault (different percentages of fault)					Without fault	With fault (different percentages of fault)				
		2%	4%	6%	8%	10%		2%	4%	6%	8%	10%
Current	1.58%	1.58%	1.59%	1.58%	1.583%	1.6%	0	0.4A	0.62A	0.73A	0.76A	0.87A
Local flux linkage	9.7%	23%	25%	34%	39%	41%	0.5 V	1.7V	1.8 V	1.8 V	1.9 V	2.1 V

As shown in Tables 2-4, it can be easily seen that the THD of stator current and the negative sequence components of the output voltage (or equivalently in the stator flux linkage) do not have a distinctive change under different loading conditions with different percentages of shorted stator windings. In fact, these results indicate the difficulty of finding clear fault signatures based on the THD of stator current and the negative sequence components of the output voltage.

Also, the amplitude of the negative sequence current rises if the percentage of shorted windings increases. In fact, different loading conditions with different percentages of shorted stator windings do not show a significant difference between the negative sequences current. On the other hand, inherent asymmetries in the machine also affect the negative sequence current component. However, for the THD analyzing, the local magnetic flux linkage is significantly affected by the fault under different conditions. As shown in Tables 2-4, it can be easily seen that the THD of local magnetic flux linkage for various operating situations has distinctive change. According to Tables 2-4, it can be clearly seen that the THD of local magnetic flux linkage has a unique behavior, so we propose the THD analyzing of local magnetic flux linkage as a suitable criterion for inter-turn fault detection.

4. DETECTION OF THE FAULTY COIL

As far as the authors are aware, most of the presented techniques do not offer the capability of identifying the specific faulty coil [3], [6]-[8], [29], [30]. On the other hand, as discussed in [31], in lap winding machine not only can faulty coil not be detected, but also, finding the faulty phase is too difficult. In lap wound machines, the electrical space phase shift between the magnetic axis of the faulty coil and the original magnetic axis of the phase winding depends on the location of the short coil, the number of coils per phase and the distribution of the coils in the stator slots. Consequently, it is difficult to detect the faulty phase in these types of machines [31]. In addition, finding clear fault signatures, in a machine equipped with the stator winding configurations of the parallel branches in internal faults is a difficult task [9]. On the other hand, along with the growth of electric power industry, investigation of fault diagnosis of

synchronous generators with several parallel paths becomes more and more significant [29]. Although the stator of studied generator in this paper has lap winding and four parallel branches in each phase, the proposed technique could identify the faulty coils under inter turn winding faults. To demonstrate the performance of the presented method, a series of actual faults of inter-turn winding fault on the aforementioned generator have been fulfilled. As representative examples of the many tests performed on the salient-pole synchronous generator in the laboratory, one illustration for each case is presented. Fig. 16a shows the forty eight voltage waveform (induced in the search coils) under no-load condition in the healthy operation. In this figure, symmetry in the magnetic field distribution under healthy operation is presented (also, see Figs. 2a and 3a). As it was mentioned earlier, under ideal conditions, the machine has an air-gap magnetic field which varies sinusoidally in space and time. Faulty operation will cause a distortion of this sinusoidal waveform. Fig. 16b shows the forty eight magnetic flux linkage waveform under no-load condition in the faulty operation. When the stator winding inter-turn fault occurs, the induced flux linkages in the search coils of the faulted area change more than those of the other search coils. Because voltage difference and circulating current will occur, the flux linkage in these areas will be most affected by this fault. In fact, in this case because the current due to the fault will change locally, the magnetic flux linkages around the faulty area will be affected by the faults. This concept is shown in Fig. 16b.

To demonstrate this concept, we have created an experimental turn-to-turn fault on the coil between the 21st and 31st slots in phase *W*, and the induced magnetic flux linkage in forty eight search coils has been measured. According to this figure, the symmetry in the magnetic field distribution is lost and induced flux linkage in search coils around two ends of the faulty coil are distorted. Induced magnetic flux linkage in these search coils have more change to induced flux linkage in other search coils, which indicates the fault has occurred in relative coils of them (also, see Fig. 2b).

In fact, according to Fig. 16b, the flux linkage adjacent to the faulty coils considerably distorts. Therefore, based on the previous discussion in sections 2 and 3, these waveforms can be analyzed using fast Fourier transform in order to extract THD because of the THD analysis of local magnetic flux linkage as a suitable criterion for inter-turn fault detection. It should be remembered that due to the effect of armature reaction under on-load conditions in the normal and faulty operations, induced magnetic flux linkage in the search coils slowly exit from the induced magnetic flux linkage in the search coils under no-load conditions (see Figs. 8, 13a and 14).

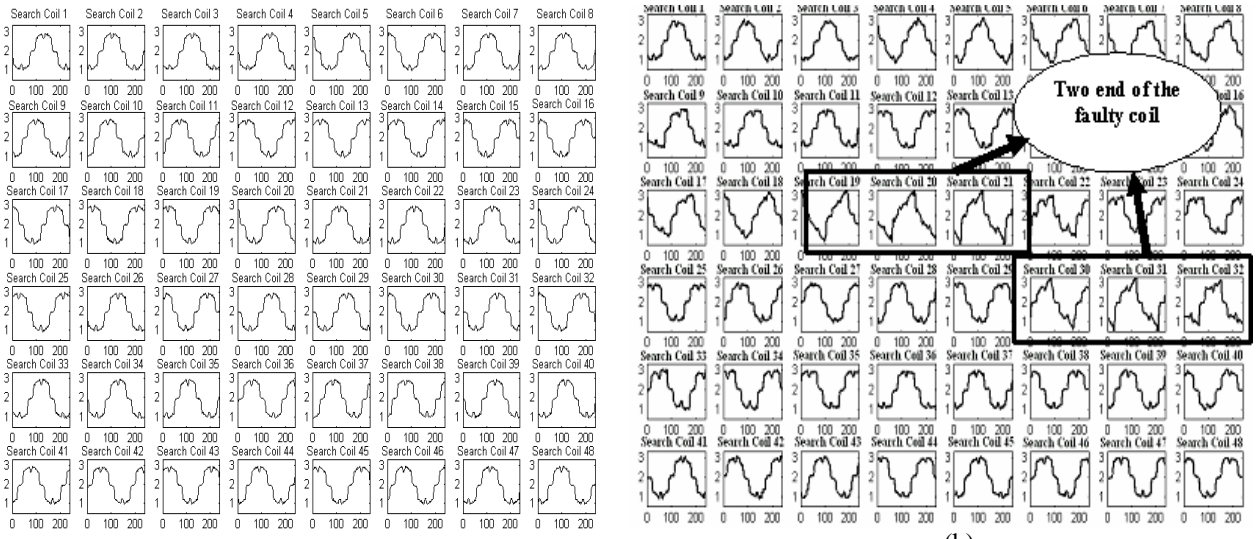

(a) (b)

Fig. 16. Forty eight measured magnetic flux linkage (a) under healthy operation (no-load). (b) Under turn-to-turn short circuit in the same branch in phase *W* (no-load)

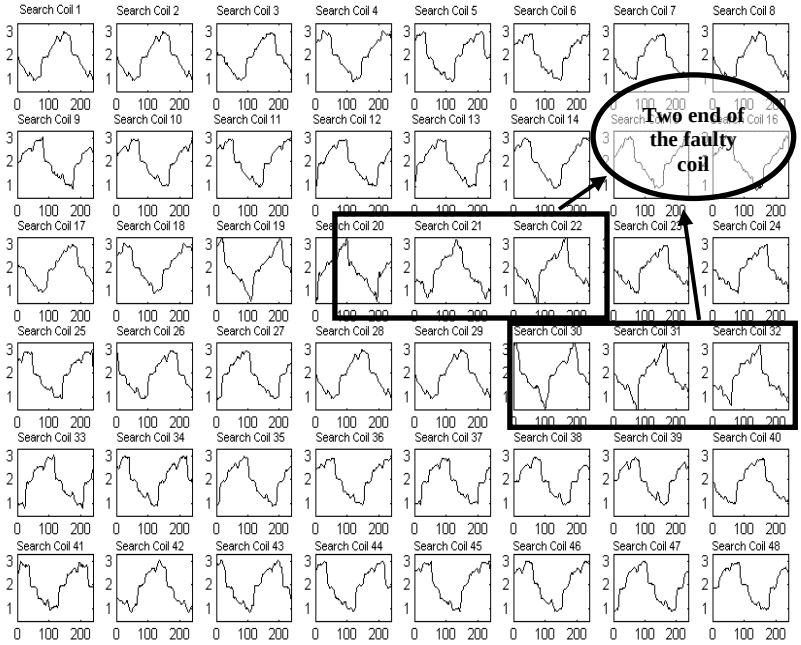

Fig. 17. Forty eight measured magnetic flux linkage under turn-to-turn short circuit in the same branch in phase W (load condition)

On the other hand, the load of synchronous generator may contain harmonics. In this condition where the generator supplies the harmonic load, different harmonics may appear within the air gap field. However, when such harmonic load exists in the air gap, detection of fault is possible. Since the harmonic content in the 48 search coils will be compared for fault detection, there should be no problem, as different loading level affects all search coils. Now consider a turn-to-turn short circuit in the winding, under this condition the harmonic content due to turn-to-turn fault will be added to the previous harmonic content due to the loading. This concept is shown in Fig.17. Fig.17 shows the forty eight voltage waveform (induced in the search coils) under load condition in the faulty operation.

5. RADIAL BASIS NEURAL NETWORK AND WAVELET ANALYSIS

In this research, the PNN and the DWT are used in the design of fault diagnosis system. In fact, in this contribution, DWT is used only for de-noising, because by reducing the noise, better network training is done. Then, FFT is used to extract the fault signature from magnetic flux linkage and a fault indicator based on THD is presented.

a) Radial basis function neural networks (RBFs)

PNN is a member of the RBFs family. The PNN is a kind of RBF suitable for classification problems. The structure of this network consists of four layers, an input, a hidden, a summation and an output layer (see Fig. 18). The input-layer neurons do not perform any computation and merely distribute input features to all the neurons in the hidden layer. The hidden layer is fully connected to the input layer. The hidden layer units represent each training set pattern and use a radial base activation function. This layer carries out a nonlinear transformation of the input space to the hidden space; the hidden space is of high dimensionality, and so transforms the nonlinear separable pattern set in linear separable output sets. In fact, neurons in the hidden layer utilize multi-dimensional kernels to estimate the probability density function (PDF) for classification [32].

In the summation layer of the PNN network, there is one neuron for each class. This layer performs an average operation of the outputs from the hidden layer for each class. Also, in the PNN network the decision layer is a competition layer. Compete transfer function in this layer picks the maximum of these probabilities, and produces a 1 for that class and a 0 for the other classes [32], [33].

The basic idea behind the PNN is a direct neural network implementation, using the Parzen nonparametric PDF estimation and the Bayes strategy for pattern classification. The Parzen estimation of the PDF for class *k* is

$$pdf_k(x) = \left(\frac{1}{2\pi^{n/2}\sigma^n}\right)\left(\frac{1}{p_k}\right)\sum_{j=1}^{p_k} e^{-(x-x_{kj})^2/(2\sigma^2)} \tag{2}$$

where x_{kj} is the j^{th} training sample from class *k*, x is the unknown input, n is the dimension number of classifying vector x, p_k is the number of training sample of class *k*, and the σ is an adjustable smoothing parameter. This equation implies that the PDF for each class can be expressed simply as the sum of the population PDFs.

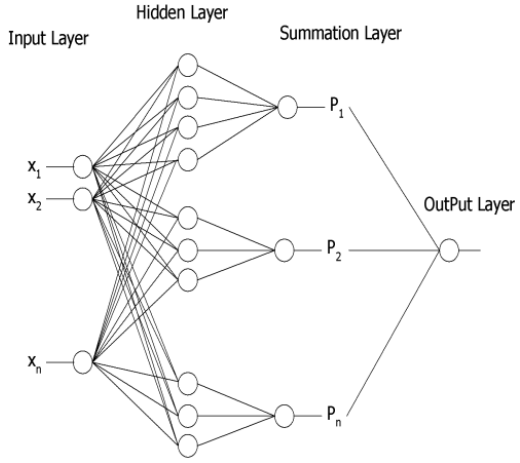

Fig. 18. The PNN neural network structure [32]

The RBF networks have some advantages over other artificial neural networks that are presented in the following [32], [33].

•The PNN learns instantaneously in one-pass through the patterns of the training set which causes them to train faster compared to other networks and these networks do not require pre-decision on the number of layers and hidden units.

•There is no need to set the initial weights and no relationship exists between learning and recalling processes in these networks.

• A PNN has got an inherently parallel structure, quick repeated iterative process and superior adaptation capability for architectural changes.

•A PNN is guaranteed to converge to a Bayesian classifier, provided that it is given enough training data.

b) Wavelet decomposition

The continuous wavelet transform (CWT) of a time-dependent signal $x(t)$ that can be defined as the sum over all time of the signal multiplied by scaled, shifted versions of the wavelet function $\psi(t)$, i.e.

$$w_x(b,a) = |a|^{-\frac{1}{2}} \int_{-\infty}^{\infty} x(t)\psi^*\left(\frac{t-b}{a}\right)dt \tag{3}$$

where $\psi(t)$ is the mother wavelet, and a and b are scale index and translation parameters, respectively.

The discrete wavelet transform (DWT) is derived from the discretization of $w_x(b,a)$ and a , b can be defined as: $a = 2^j$, $b = 2^j k$, $j,k \in z$. Therefore, by using (3), the discrete wavelet transform can be expressed as follows:

$$DWT(j,k) = \left|2^j\right|^{-\frac{1}{2}} \int_{-\infty}^{\infty} x(t)\psi^*(\frac{t-2^j k}{2^j})dt \tag{4}$$

Many applications use the wavelet decomposition. One of the most popular applications of the wavelet transforms is in de-noising studies on the steady state problems [34]. The aim of de-noising is to eliminate the noise and to retain the important features as much as possible. In recent times, signal de-noising studies using nonlinear processing, such as wavelet transformation, have become increasingly popular [34]. In this project, DWT based on the filtering scheme illustrated in Fig. 19 is used for de-noising, since by reducing the noise, better network training is done. The fundamental idea of the wavelet analysis is that the original signal, $x(t)$, passes through two complementary filters and is decomposed into approximation coefficients representing low-frequency components ($A's$) and detail coefficients representing high frequency components ($D's$).

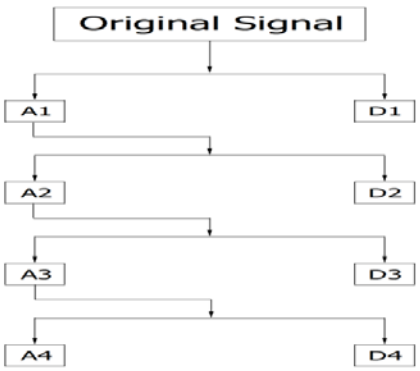

Fig. 19. Tree of four levels DWT decomposition of an original signal [34]

When the "mother" wavelet is selected, the corresponding scaling-filters are defined from which associated low-pass and high-pass filters are computed [33]. The general de-noising is carried out by the following three steps [33], [35]. It can be briefly described as follows: 1) Select a wavelet, select a level N and decompose the original signal at level N into approximation and detail coefficients using the DWT. 2) Threshold detail coefficients. Modify the detail coefficients at each level by applying soft thresholding to the detail coefficients. 3) Reconstruct the de-noised signal. Calculate wavelet reconstruction using the original approximation coefficients of level N and the modified detail coefficients of levels from 1 to N.

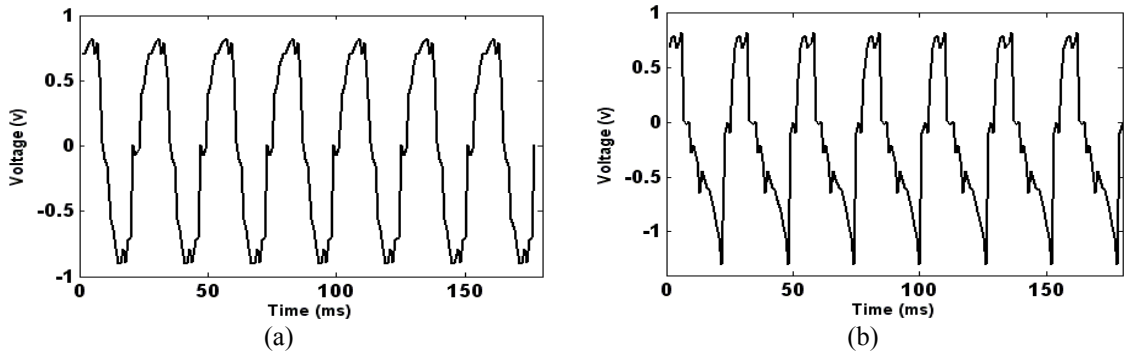

(a) (b)

Fig. 20. The voltage induced in a search coil. (a) Under healthy operation. (b) Under faulty operation

To effectively implement the de-noising procedure, it is necessary to select the suitable "mother" wavelet and "thresholding". In this research extensive testing with different kinds of mother wavelets show that the discrete meyer wavelet transform is the most appropriate wavelet.

In order to show the Performance of the utilized DWT in noisy environment, in the following the problem of signal recovery from noisy data is presented. The underlying model for the noisy signal is basically of the following form:

$$s(n) = f(n) + \delta\, e(n) \tag{5}$$

where time n is equally spaced.

In the model it is supposed that e(n) is a Gaussian white noise and the noise level δ is supposed equal to 1. The de-noising objective is to suppress the noise part of the signal and to recover f (n). Fig.20 shows the simulation stator teeth voltages (induced in a search coil) at steady state condition under healthy and faulty operations at no-load.

First, white Gaussian noise is added to these signals (signal f (n)). Then, based on previous discussion (three steps in de-noising), signal recovery from noisy data (polluted signal) is presented.

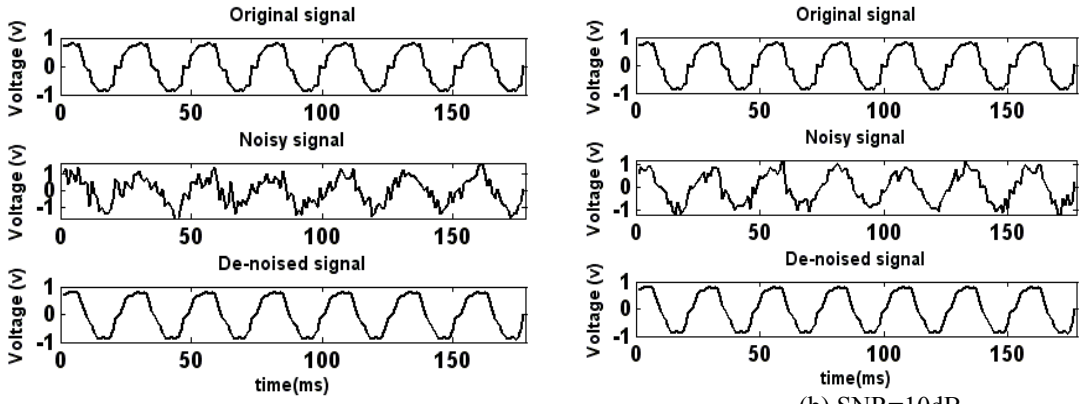

(a) SNR=5dB (b) SNR=10dB

Fig. 21. Induced voltage in a search coil under normal operation. (a) Original signal corrupted with Gaussian white noise with SNR=5dB. (b) Original signal corrupted with Gaussian white noise with SNR=10dB

Figure 21a shows induced voltages in a search coil (original signal), corrupted induced voltages with Gaussian white noise with SNR=5dB (noisy signal) and de-noised signal of the original waveform using discrete meyer wavelet transform respectively under normal operation. Similarly, Fig. 21b represents the above described characteristics for the corrupted induced voltages in a search coil with Gaussian white noise with SNR=10dB (noisy signal) under normal operation.

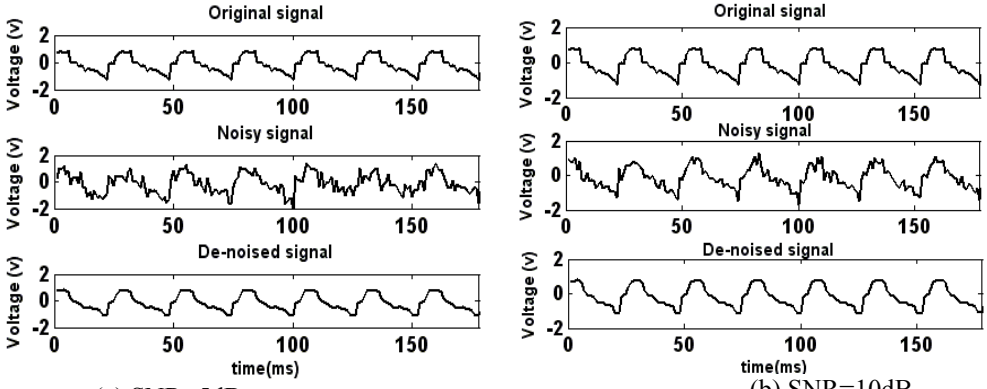

(a) SNR=5dB (b) SNR=10dB

Fig. 22. Induced voltage in a search coil under faulty operation. (a) Original signal corrupted with Gaussian white noise with SNR=5dB. (b) Original signal corrupted with Gaussian white noise with SNR=10dB

On the other hand, Fig. 22a shows original signal, noisy signal corrupted with Gaussian white noise with SNR=5dB and de-noised signal of the original waveform using discrete meyer wavelet transform respectively under faulty operation. Similarly, Fig. 22b represents the above described characteristics for the corrupted induced voltages in a search coil with Gaussian white noise with SNR=10dB (noisy signal) under faulty operation. As stated earlier, the aim of de-noising is to eliminate the noise and to retain the important features as much as possible. As it is seen from these figures, de-noising eliminates the high frequency component and the main structures of the original signals are retained so that de-noising will help to improve the classification performance.

c) Design of fault diagnosis system with the aid of neural network

PNN as the main part of this fault diagnosis system and DWT are combined effectively to construct the classifier. In this research DWT is used only for de-noising. Then, FFT is used to extract the fault signature from magnetic flux linkage and a fault indicator based on THD is presented.

As stated earlier, in the proposed method the main criterion is THD of local magnetic flux linkage. The THD of local magnetic flux linkage is insignificant in case of normal operation, but it increases in the case of inter turn winding faults. For the proposed method, extensive tests show that if the THD of local magnetic flux linkage is less than 10%, the setting will be acceptable and the no fault has happened (so THD setting $\leq 10\%$). In fact, in normal operations the THD of local magnetic flux linkage is less than 10%. Also, if the THD of local magnetic flux linkage increased more than 10 percent, the setting will be acceptable and the inter turn winding fault has happened (so THD setting>10%). For better illustration, Table.5 explores the distinction between different conditions. In fact, fault distinction is summarized in this Table.

Table 5. Criteria for the distinction between different conditions in the proposed method

Fault code	Fault type	THD setting
1	No fault (normal)	THD $\leq 10\%$
2	Turn-to-turn fault	THD $>10\%$

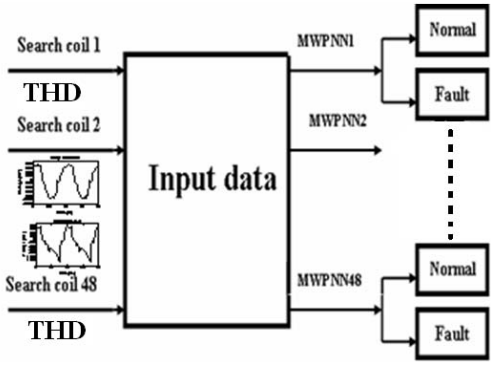

Fig. 23. Procedure for detection of faulty coil by MWPNN

In the following, procedure for detection of faulty coil by PNN based on the previous discussion and the experimental results is presented. Forty eight search coils are sampled simultaneously in one or more cycles (depending on the used hardware). Therefore, a vector of sets are obtained. The obtained waveforms are analyzed by discrete wavelet transform and de-noised signals are extracted. These waveforms will be analyzed using fast Fourier transform in order to extract the THD. Then PNN is trained by THD extracted from the magnetic flux linkage data. In this scheme, regarding the number of search coils, forty eight MWPNN are used for detection of faulty coils. Each MWPNN is carried out only for two classes i.e., normal and fault for the classification. When no faults are present in the generator, all MWPNN's will predict the normal class. If some MWPNN's predict the fault class, the turn-to-turn short

circuit has occurred. This process is illustrated in Fig. 23. Also, Table 6 lists the parameters of the MWPNN in this procedure for detection of faulty coil.

Table. 6. Parameters of the MWPNN for detection of the faulty coil

Method	Related parameter		
PNN	Input layer	240	nodes (depending on the used hardware)
	Output layer	2	nodes
	Smoothing parameter	0.5	

Each neural network is trained with 5 input data of each class (10 input data for two classes) and 20 data of each class are considered for testing (40 test data for two classes). These data for training and testing phases are independent. It must be noted that PNN learns quickly in one-pass through the patterns of the training set and it is known that the training speed of PNN over back propagation networks is high. In PNN, training speed is approximately seven times faster than BP [36], [37] and PNN doesn't need pre-decision on the number of layers and hidden units. The training procedure of PNN networks is usually performed in two stages: 1) the centre and standard deviation of the Gauss function are chosen; 2) the weights related to the connections among the hidden units and the output units are fixed [38].

In fact, a serious aspect of the training procedure is mainly represented by efficient choice of the centre and standard deviation of the Gauss function, as this selection may strongly affect errors made by the classifier [38]. Consequently, in design of the MWPNN it is very important to select an optimal value of the smoothing parameter. Procedure of classifying starts with finding the optimal smoothing value for MWPNN. If smoothing value is near zero, the network acts as a nearest neighbor classifier. As smoothing value becomes larger, the designed network takes into account several nearby design vectors. In this research, the traditional trial and error method is used to obtain optimum smoothing factor. Also, care must be taken in choosing data for obtaining a good training set in order to increase the performance of a neural network.

To evaluate the performance of MWPNN, its results are compared with different artificial neural networks. These different networks are trained and subsequently tested with the same data due to a similar procedure that has been mentioned before. First fault diagnosis system uses BP neural network. The second system uses PNN and the third system uses MWPNN. It must be noted that backpropagation neural network is most widespread among all artificial neural networks. These networks are also referred to as multilayered perceptron (MLP) or feedforward networks.

Table. 7. Diagnosis accuracy for test results

ANN	MLP	PNN	MWPNN
Classification accuracy	55%	78%	$\geq 95\%$

The multilayered perceptron neural network is trained with the Batch Gradient Descent with Momentum. In detection of faulty coil, for the MLP neural network, several network configurations were tried, and better results have been obtained by a network constituted by three layers with 240, 24, and 2 neurons. Sigmoid is selected as the act function of neurons in every layer. The results of comparison for detection of faulty coil are presented in Table.7. In the testing process, the results of 18 testing samples were wrong in MLP neural network. So, the accuracy is 55% (22/40). The accuracy of normal PNN neural network is around 78% (31/40) because the results of 9 testing samples were wrong in PNN network. Also, the results of 2 testing samples were wrong in MWPNN neural network. So, the accuracy is 95% (38/40). It's worth mentioning that, the training set influences the performance of these neural networks. However extensive test show that the accuracy of MWPNN network is higher than other networks.

6. CONCLUSION

Results under different conditions are presented and analyzed. In this paper, it is shown that the magnetic flux linkage is a suitable criterion for the detection of turn-to-turn winding faults. FFT is used to extract the fault signature from magnetic flux linkage and by analyzing this signal, inter-turn faults have been detected. The main feature of the proposed method is its ability to identify the faulty coils under turn-to-turn winding faults. Simple algorithm, low cost sensor and sensitivity are the other features in the proposed technique.

NOMENCLATURE

Variables

x_{kj}	j^{th} training sample from class k
x	unknown input
n	dimension number of classifying vector x
P_k	number of training sample of class k
σ	adjustable smoothing parameter
φ_F	flux produced by the rotor field winding
φ_{ar}	flux produced by the stator current
φ_{ag}	resultant flux

Abbreviations

EMF	electromotive force
FEM	finite element method
FFT	fast Fourier transforms
PDF	probability density function
PF	power factor
RMS	root mean square
THD	total harmonic distortion
MMF	magneto motive force
SNR	signal to noise ratio
DWT	discrete wavelet transform
PNN	probabilistic neural network
MLP	multilayered perceptron

REFERENCES

1. Vahedi, A. & Behjat, V. (2011). Online monitoring of power transformers for detection of internal winding short circuit faults using negative sequence analysis. *European Transactions on Electrical Power*, Vol. 21, No. 1, pp. 196–211.
2. Dehghani, M. & Karrari, M. (2007). Nonlinear robust modeling of synchronous generators. *Iranian Journal of Science and Technology, Transaction B: Engineering*, Vol. 31, No. B6, pp. 629-640.
3. Tu, X., Dessaint, L. A., Kahel, M. E. & Barry, A. O. (2006). A new model of synchronous machine internal faults based on winding distribution. *IEEE Transactions on Industrial Electronic*, Vol. 53, No. 6. pp. 1818-1828.
4. Mirafzal, B., Povinelli, R. J. & Demerdash, N. A. O. (2006). Inter-turn fault diagnosis in induction motors using the pendulous oscillation phenomenon. *IEEE Transactions on Energy Conversion*, Vol. 21, No. 4, pp. 871–882.
5. Penman, J. & Jiang, H. (1996). The detection of stator and rotor winding short circuits in synchronous generators by analysing excitation current harmonics. *International Conference on Opportunities and Advances in International Electric Power Generation*, Durham, UK, pp. 137-142.
6. Bei, O., Xiangheng, W., Yuguang, S., Weijian, W. & Weihong, W. (2000). Research on the internal faults of the salient-pole synchronous machine. *IEEE, Power Electronics and Motion Control Conference, Proceedings. PIEMC*. The Third International, pp.558-563.

7. Wang, X. H., Sun, Y. G., Ouyang, B., Wang, W. J., Zhu, Z. Q. & Howe, D. (2002). Transient behaviour of salient-pole synchronous machine with internal stator winding faults. *Proc. Inst. Electr. Eng.—Electr. Power Appl*., Vol. 149, No. 2, pp. 143–151.
8. Lin, X., Tian, Q., Gao, Y. & Liu, P. (2007). Studies on the internal fault simulations of a high-voltage cable-wound generator. *IEEE Transactions on Energy Conversion*, Vol. 22, No. 2, pp. 240–249.
9. Negrea, M. D. (2007).Electromagnetic flux monitoring for detecting faults in electrical machines. Ph.D. dissertation, Helsinki University of Technology, Laboratory of Electromechanics, Helsinki, Finland, The dissertation can be read at http://lib.tkk.fi/Diss/isbn9512284774.
10. Thomson, W. T. (1999). A review of on-line condition monitoring techniques for three-phase squirrelcage induction motors–past, present and future. *2nd IEEE International Symposium on Diagnostics for Electrical Machines, Power Electronics and Drives–SDEMPED*, Spain, pp. 3-17.
11. Burnett, R. & Watson, J. F. (1995). The current analysis program-a software tool for rotor fault detection in three phase induction motors. *7th International Conference on Electrical Machines and Drives*, Durham, UK, pp. 156-160.
12. Payne, B. S., Husband, S. M. & Ball, A. D. (2002). Development of condition monitoring techniques for a transverse flux motor. *International Conference on Power Electronics, Machines and Drives–PEMD '02 (IEE Conference Publication No. 487)*, Bath, UK, pp. 139-144.
13. Yaghobi, H., Mashhadi, H. R. & Ansari, K. (2011). Artificial neural network approach for locating internal faults in salient-pole synchronous generator. *ELSEVIER, Expert Systems with Applications,* Vol. 38, pp. 13328–13341.
14. Yaghobi, H., Mortazavi, H., Ansari, K., Rajabi Mashhadi, H., Khorashadi zadeh, H. & Borzoe, H. (2012). Study on application of flux linkage of synchronous generator for loss of excitation detection. *European Transactions on Electrical Power, Published online in Wiley Online Library.* DOI: 10.1002/ETEP.1626.
15. Yaghobi, H., Ansari, K. & Mashhadi, H. R. (2011). Analysis of Magnetic Flux Linkage Distribution in Salient-Pole Synchronous Generator with Different Kinds of Inter-Turn Winding Faults. *Iranian Journal of Electrical & Electronic Engineering*, Vol. 7, No. 4, pp. 260-272.
16. Yaghobi, H., Mortazavi, H., Ansari, K., Mashhadi, H. R., Zade, H. K. & Borzoe, H. (2010). A Novel Flux-Based Method for Synchronous Generator Loss of Excitation Protection. *25th International Power System Conference*; Iran.
17. Bui, V. P., Chadebec, O., Rouve, L. L. & Coulomb, J. L. (2008). Noninvasive fault monitoring of electrical machines by solvingthe steady-state magnetic inverse problem. *IEEE Transactions on Magnetics*, Vol. 44, No. 6, pp. 1050–1053.
18. Henao, H., Demian, C. & Capolino, G. A. (2003). A frequency-domain detection of stator winding faults in induction machines using an external flux sensor. *IEEE Transactions on Industry Applications*, Vol. 39, No. 5, pp. 1272- 1279.
19. Assaf, T., Henao, H. & Capolino, G. A. (2004). Simplified axial flux spectrum method to detect incipient stator inter-turn short-circuits in induction machine. *IEEE International Symposium on Industrial Electronics*, Vol. 2, pp. 815- 819.
20. Han, S. B., Hwang, D. H., Yi, S. H. & Kang, D. S. (2008). Development of diagnosis algorithm for induction motor using flux sensor. *International Conference on Condition Monitoring and Diagnosis*, Beijing, China.
21. Nandi, S., Toliyat, H. A. & Li, X. (2005). Condition monitoring and fault diagnosis of electrical machines- A Review. *IEEE Transactions on Energy Conversion*, Vol. 20, No. 4, pp. 719–729.
22. Stone, G. C., Boulter, E. A., Culbert, I. & Dhirani, H. (2004). *Electrical insulation for rotating machines.* John Wiley & Sons Publishers, IEEE Press, the Institute of Electrical and Electronics Engineers, New York, pp. 12–20, ISBN: 0-471-44506-1.

23. Luo, X., Liao, Y., Toliyat, H. A., Antably, A. El. & Lipo, T. A. (1995). Multiple coupled circuit modeling of induction machines. *IEEE Transactions on Industry Applications*, Vol. 31, No. 2, pp. 311-318.
24. Negoita, A., Scutaru, Gh. & Ionescu, R. M. (2010). A brief review of monitoring techniques for rotating electrical machines. *Bulletin of the Transilvania University of Brasov*, Vol. 3, No. 52, Series I: Engineering Sciences.
25. Xuan, M. T., Simond, J. J., Wetter, R. & Keller, S. (2006). A novel air-gap monitoring system for large low speed hydro-generators. *IEEE, Power Engineering Society General Meeting*, pp. 1–8.
26. Cabanas, M. F., Glez, F. P., González, M. R., Melero, M. G., Orcajo, G. A., Cano, J. M. & Rojas, C. H. (2005). A new on-line method for the early detection of broken rotor bars in asynchronous motors working under arbitrary load conditions. *Industry Applications Conference, Fourtieth IAS Annual Meeting*, Vol. 1, pp. 662–669.
27. Chari, M. V. K. (1974). Nonlinear finite element solution of electrical machines under no-load and full-load conditions. *IEEE Transactions on Magnetics*, Vol. 10, No. 3, pp. 686-689.
28. Cruz, S. M. A. & Cardoso, A. J. M. (2003). Diagnosis of stator inter-turn short circuits in DTC induction motor drives. *IEEE Industry Applications Conference*, 38th IAS Annual Meeting, Vol. 2, pp. 1332–1339.
29. Megahed, A. I. & Malik, O. P. (1999). Simulation of internal fault in synchronous machines. *IEEE Transactions on Energy Conversion*, Vol. 14, No. 4, pp. 306-1311.
30. Muthumuni, D., Mclaren, P. G., Dirks, E. & Pathirana, V. (2001). A synchronous machine model to analyze internal faults. *IEEE Industry Applications Conference*, 36th IAS Annual Meeting, Vol. 3, pp. 1595-1600.
31. Ahmed, A. S., Yeh, C. C., Demerdash, N. A. O. & Mirafzal, B. (2006). Analysis of stator winding inter-turn short-circuit faults in induction machines for identification of the faulty phase. *IEEE, Industry Applications Conference*, 41st IAS Annual Meeting, Vol. 3, pp. 1519–1524.
32. Picton, P. (2000). *Neural networks*. Palgrave Macmillan Publisher, pp. 102–109, ISBN: 780333948996.
33. Gerbec, D., Gasperic, S., Smon, I., Gubina, F. (2005). Allocation of the load profiles to consumers using probabilistic neural networks. *IEEE Trans.Power Systems*, Vol. 20, No. 2, pp. 548-555.
34. Hu, W. B., Li, K. C., Zhao, D. J. & Xie, B. R. (2007). Performance improvement of power quality disturbance classification based on a new de-noising technique. *IEEE, Proceedings of the International Conference on Electrical Machines and Systems*, Seoul, Korea.
35. Misiti, M., Misiti, Y., Oppenheim, G. & Poggi, J. M. (2002). *Wavelet toolbox for use with matlab*. Natick, MA: Mathworks.
36. Specht, D. F. & Shapiro, P. D. (1991). Generalization accuracy of probabilistic neural networks compared with back-propagation networks. *IEEE, International Joint Conference on Neural Networks*, Vol. 1, pp. 887-892.
37. Farrokhrooz, M. & Karimi, M. (2006). A performance comparison between conventional PNN and multi-spread PNN in ship noise classification. *IEEE, International Joint Conference on OCEANS-Asia pacific*, pp. 1-4.
38. Bruzzone, L. & Prieto, D. F. (1998). Supervised training technique for radial basis function neural networks. *Electronics letters* 28th, Vol. 34, No. 11, pp. 1115-1116.